Korean J. Chem. Eng., 37(12), 2287-2294 (2020)
DOI: 10.1007/s11814-020-0649-4

pISSN: 0256-1115
eISSN: 1975-7220

Mixed matrix composite membranes based on amination of reduced graphene oxide for CO_2 separation: Effects of heating time and nanofiller loading

Gishedaraankumar Krishnan*, Safia Syazana Mohtar, Farhana Aziz*,**,†, Juhana Jaafar*,**, Norhaniza Yusof*,**, Wan Norharyati Wan Salleh*,**, and Ahmad Fauzi Ismail*,****

*School of Chemical and Energy Engineering, Faculty of Engineering, Universiti Teknologi Malaysia, 81310 Johor Bahru, Johor, Malaysia
**Advanced Membrane Technology Research Centre (AMTEC), Universiti Teknologi Malaysia, 81310 Johor Bahru, Johor, Malaysia
(*Received 21 April 2020 • Revised 28 July 2020 • Accepted 31 July 2020*)

Abstract−The CO_2 gas separation performance of aminated reduced graphene oxide (A-rGO) incorporated PEBAX mixed matrix composite membranes, by means of amination heating time and A-rGO loading, is reported. The 5 h of heating time resulted in an essential molecular sieving property for CO_2 separation, thus used in membrane fabrication. The selective PEBAX/A-rGO5 layers were fabricated on top of the polysulfone supporting layer by a dip-coating method. The A-rGO was well-dispersed, the selective and support layers were seamlessly attached. The CO_2 permeability and CO_2/N_2 selectivity of the PEBAX/A-rGO5 was greater than that of pristine PEBAX. 3 wt% of A-rGO5 loading resulted as the optimum since the gas selectivity decreased at higher loading. The PEBAX/A-rGO5 performance, which was slightly above the Robeson 2008 upper bound of permeability-selectivity relation for CO_2/N_2 gas separation, shows a promising application for industrial CO_2 gas separation process.

Keywords: Aminated Reduced-Graphene Oxide, CO_2 Selective Membrane, Gas Separation Process, Mixed Matrix Membrane, PEBAX

INTRODUCTION

Tremendous development of the carbon dioxide (CO_2) gas separation membrane in both academia and industry is evident since the discovery of asymmetric membranes by Loeb and Sourirajan in 1964 [1]. Many new membrane materials have been introduced and verified to accommodate the latest industrial needs. Polymers, nonetheless, are the leading membrane material owing to their cost-effectiveness, processability, and durability [2,3]. Despite the current proliferation of newly researched and developed polymers, the renowned permeability and selectivity "trade-off", as indicated by the Robeson plot, limit their success on a large-scale industrial application [2,4]. Furthermore, industrially available membranes for CO_2 separation process are demanded to have high durability, plasticization and performance stability, high chemical resistance, and low-cost [5,6]. These issues and requirements have driven researchers to come up with new strategies of combining the benefits of the economical processability polymer with high selectivity inorganic materials, known as mixed matrix membranes (MMMs).

MMMs are designed to display the best characteristics of the component materials for enhanced permeability and insignificant drop in the selectivity. The selection of polymers should contain functional groups with affinity towards CO_2 molecules to promote adsorption. The most common polymeric materials that have been actively studied include polysulfones (Psf) [7,8], polycarbonates [9], poly(aryletherketones) [10,11], polyethersulfone [12], cellulose acetate [13], polyvinylamines [14], polyvinylacetates [15] and polyimides [11,16]. They have been studied primarily due to their superior performance regarding CO_2 gas permeability and selectivity. Another promising polymeric material for CO_2 gas separation, namely, poly(ether block amide) (i.e., PEBAX) has also been studied [17-19]. Its exceptional film forming characteristics, composition of hard segments polyamide (PA) that contributes to its mechanical strength, and soft segment polyether with large pore volume for transport channel makes this co-polymer particularly valuable.

Inorganic fillers, on the other hand, modify the microstructure of the membrane matrix, influencing the free volume distribution and hindering densification of the polymer matrix [20]. A complementary combination of polymer and inorganic materials not only yields high CO_2 diffusivity or permeability but also delays the plasticization phenomenon [21,22]. However, to achieve the ideal MMMs is nonetheless challenging. Homogeneous dispersion of particles, defect-free interface, and organic/inorganic materials compatibility have been critical issues in MMMs development.

Selection of suitable inorganic materials is undeniably a matter of concern. Inorganic materials, such as zeolites [7], mesoporous silica [8], silica nanospheres [23], carbon molecular sieves [24], carbon nanotubes [10,16], and metal organic frameworks [15], have been tested to prepare the MMMs. The addition of these fillers by a small fraction into the polymer matrix could considerably increase the overall CO_2 separation performance. Nowadays, graphene-based materials have gained much attention for membrane preparation

†To whom correspondence should be addressed.
E-mail: farhanaaziz@utm.my

due to their two-dimensional morphology and tunable physicochemical characteristics. Among various graphene-based materials, graphene oxide (GO) shows remarkable solution processability, which allows simple processing into continuous films and compliance integration with the existing membrane fabrication techniques [25,26]. In MMMs study for CO_2 gas separation, GO has been widely applied by incorporating directly into polymer [27], chemically modified into a nanosheet filler [28], a grafted nanofiller [29], and a reduced GO filler [30] prior blending with polymer, and fabricated as nanosheet selective layer [31].

In our previous work, GO was incorporated with PEBAX as the selective layer, supported by Psf porous membrane [32]. The GO was partially reduced prior to amination resulting in CO_2 permeability of 47.50 Barrer with CO_2/N_2 and CO_2/CH_4 selectivity of 105.60 and 23.75, respectively. Encouraged by the findings, despite partially reduced GO, we synthesized an aminated reduced graphene oxide (A-rGO) to be incorporated with PEBAX for CO_2 gas separation performance test. To the best of our knowledge, there are no reports on A-rGO as filler in a selective layer of mixed matrix composite membranes (MMCMs) for CO_2 separation processes. The GO was fully reduced by heating during the amination process and characterized by the crystallinity and functional group studies. A porous Psf membrane supported the thin selective layer on-top through a dip-coating technique. The loading of A-rGO was manipulated and the fabricated MMCMs were characterized by means of morphology, functional groups, and T_g studies. The CO_2 gas performance indicated by gas permeability and selectivity was investigated through a single gas permeation experiment.

EXPERIMENTAL

1. Materials

PEBAX (MH1657) was obtained from Arkema (France). Ammonium hydroxide (NH_4OH, 25 vol%), hydrochloric acid (HCl, 37% ACS reagent), Psf (Udel-P1700), and sodium bisulfite ($NaHSO_3$, ACS reagent) were purchased from Sigma-Aldrich (USA). Graphite powder (Ø<20 μm) was obtained from Merck KGaA (German). Dimethylformamide (DMF, ≥99% reagent grade), and hydrogen peroxide (H_2O_2, 30% certified ACS) were supplied by Fisher Scientific (USA). Sulfuric acid (H_2SO_4, 95-98%, A.R./ACS) and potassium permanganate ($KMnO_4$, C.P.) were obtained from R&M Chemicals (India). Sodium nitrate ($NaNO_3$, ChemAr) was purchased from SYSTERM (Malaysia). CO_2 (99.99%), methane (CH_4, 99.99%), and nitrogen (N_2, 99.99%) gases were obtained from Mega Mount Industrial Gases Sdn. Bhd. (Malaysia). All chemicals were used as received.

2. Preparation of A-rGO

8 g graphite oxide and 4 g $NaNO_3$ was added into a beaker in an ice bath followed by 184 mL H_2SO_4 under stirring. The mixture was kept stirred for 15 min. Then, 24 g $KMnO_4$ was added slowly to the mix while maintaining the reaction temperature below 20 °C. The resulting slurry was stirred for 2 h at 300 rpm before being transferred to a hot water bath at 40 °C and continued to be stirred for 30 min at 500 rpm. The temperature of the mixture was then increased to 84 °C by slowly adding 400 mL of hot water. The mixture was stirred for 20 min prior to quenching rapidly with 1,200 mL water and stirred for 45 min. Then, 90 mL of H_2O_2 was added dropwise to stop the reaction, in which the color of the mixture changed from dark brown to yellowish-brown. The mixture was stirred for 30 min before left overnight to allow precipitation. The precipitate was filtered and washed three times with 7 vol% HCl solution diluted in deionized water before washing with deionized water until pH 6 was obtained. The solid, which was GO, was dried in a vacuum oven at 45 °C overnight.

0.15 g of the GO was sonicated in 150 mL of demineralized water and then stirred for 1 h before being transferred to a hydrothermal autoclave tube. 10 mL of 25 vol% NH_4OH solution and 3 g $NaHSO_3$ was added into the GO solution and heated at 170 °C for 3 h, 5 h, and 10 h. The solution was filtered, and the solid, which was A-rGO3, A-rGO5, and A-rGO10, respectively, was washed with demineralized water five times to remove the remaining NH_4OH and $NaHSO_3$. The A-rGOs were dried in an oven at 60 °C for 3 h and stored in a tightly capped container.

Table 1. Formulation of dope solutions

Sample	Psf (wt%)	PEBAX (wt%)	GO (wt%)	A-rGO (wt%)
PEBAX	19	4	0	0
PEBAX/GO	19	4	0.1	0
PEBAX/A-rGO5-0.1	19	4	0	0.1
PEBAX/A-rGO5-0.3	19	4	0	0.3
PEBAX/A-rGO5-0.5	19	4	0	0.5

3. Fabrication of PEBAX-based MMCMs

The PEBAX-based MMCMs were fabricated by coating a selective layer over a supporting substrate layer. The formulation is shown in Table 1. The support layer dope was prepared by dissolving 19 wt% Psf in DMF under mixing for overnight to obtain a homogeneous solution. The dope was cast via phase inversion casting technique on a glass plate before being immersed in a coagulation bath for 24 h to obtain a porous flat sheet membrane.

The selective layer dope was prepared by first dissolving the inorganic fillers (i.e., GO and A-rGO) in ethanol/water solution (70 : 30, w/w) under sonication for 1 h prior to stirring for 15 min. The PEBAX, in the meantime, was dissolved in the same type of solvent under reflux at 80 °C for 2 h. Then, the filler solution was added slowly into the PEBAX dope and stirred under reflux at 80 °C for 6 h.

The PEBAX/filler dope was then poured onto a petri dish just enough to cover the bottom surface. Then, one side of the flat sheet Psf membrane was immersed in the dispersed PEBAX/filler dope. The immersed membrane was then dried in ambient for 6 min before being immersed again in the same dope, then dried again in ambient for 12 h.

4. Characterization Procedures

The physicochemical properties of the synthesized A-rGOs and fabricated PEBAX and PEBAX-based MMCMs were characterized. X-ray diffractometer model PANalytical X'Pert Pro (UK) was used to study the crystallinity of the synthesized A-rGOs. The XRD imaging was recorded at the emission current of 40 mA, accelerating voltage of 40 kV, and Cu-Kα radiation (λ=0.154 nm) over the 2θ angle scanning from 5° to 50°. The interlayer spacing of the crys-

tal, d (nm), was determined using Bragg's equation as shown in Eq. (1)

$$d = \frac{\lambda}{2\sin\theta} \quad (1)$$

where λ (nm) is the wavelength of the incidents x-rays and θ (°) is the angle of responding peak. PerkinElmer Spectrum One (USA) infrared spectrometer was used to investigate the functional groups of the synthesized A-rGOs, PEBAX, and PEBAX-based MMCMs in the range of 4,000 cm^{-1} to 500 cm^{-1} with 64 scans and a resolution of 2 cm^{-1}. The T_g of the membranes was measured using Perkin-Elmer Simultaneous Thermal Analyzer (STA) 8000 (USA) with differential scanning calorimetry (DSC) mode under N_2 atmosphere in the range of 40 °C to 250 °C with a scanning speed of 10 °C min^{-1}. The morphology of the fabricated membranes was characterized using SEM model Hitachi Backscatter Detector S-3000 (Japan). The membrane samples were fractured in liquid nitrogen before being sputtering with gold as the preparation for the analysis.

5. Gas Permeation Test

Single gas permeation experiments were carried out on an in-house stainless-steel permeation apparatus with an effective area of 19.64 cm^2. The permeation cell was sealed with O-ring to prevent gas leakage at high pressure. The permeability of N_2, CH_4, and CO_2 gases was measured at a transmembrane pressure of 4 bar at room temperature in sequence. An amount of the same tested gas was purged first into the cell before the experiment to eliminate traces of the previously tested gas in the cell compartment. A simple soap bubble flow meter was used to obtain the flow rate of the permeating gas as well as permeability and selectivity of the membrane. For each membrane sample, its gas permeates volumetric flowrate was measured five times and the gas permeability, P (Barrer), was calculated using Eq. (2)

$$P = LP = \left(\frac{L}{A(p_i^p - p_i^f)}\right)Q \quad (2)$$

where L is the membrane thickness (m), A is the membrane area (m^2), Q is the permeate volumetric flowrate (mol s^{-1}), p_i^p, and p_i^f are the respective absolute pressure of component i on the feed side and permeate side of the membrane. The membrane separation capability or selectivity is expressed as the ratio of the permeances or permeabilities of components *i* and *j*. It was calculated using Eq. (3)

$$\alpha_{ij} = \frac{\frac{P_i}{l}}{\frac{P_j}{l}} = \frac{P_i}{P_j} \quad (3)$$

where α_{ij} is the selectivity of the membrane for component *i* over component *j*.

RESULTS AND DISCUSSION

1. Characterization of A-rGO

The XRD patterns of GO and A-rGOs are presented in Fig. 1. It was observed that the XRD pattern of GO was similar to the result by Mohammed et al. [32]. For the A-rGO3, A-rGO5, and A-rGO10, the absence of a peak at 11°, which exists in GO pattern, indicates the reduction of GO. A shifting peak observed at 6°, 5.3°, and 4.9°, for A-rGO3, A-rGO5, and A-rGO10, respectively, relates to the longer interplanar distance of graphene due to amine chains. A broad peak observed at 24.6° (d=0.370 nm), 26.7° (d=0.343 nm) and 28.3° (d=0.325 nm) is due to the aggregation or restacking of A-rGO sheets [32,33]. Since d-spacing of the A-rGOs is expected to assist in playing out of separating CO_2 from a mixture of gases, it is important to determine the suitable A-rGO as a membrane filler. From the XRD analysis, it was discerned that the interplanar spacing of A-rGO5 was bigger than the dynamic diameter value of CO_2 gas (0.340 nm) but smaller than that of N_2 (0.363 nm) and CH_4 (0.380 nm) gases. Thus, A-rGO5 was selected for further membrane fabrication.

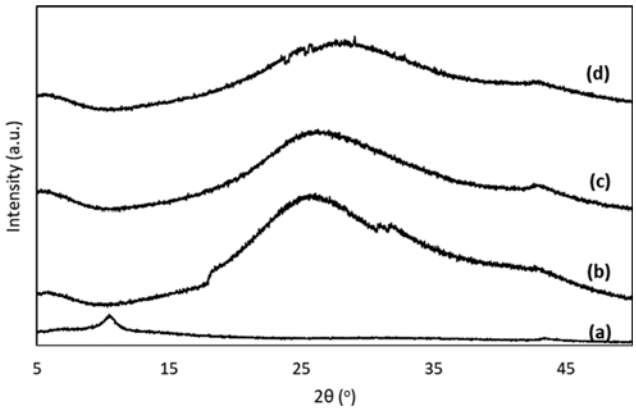

Fig. 1. XRD of patterns of (a) GO, (b) A-rGO3, (c) A-rGO5, and (d) A-rGO10.

The FTIR spectra of A-rGOs, as shown in Fig. 2, elucidate the

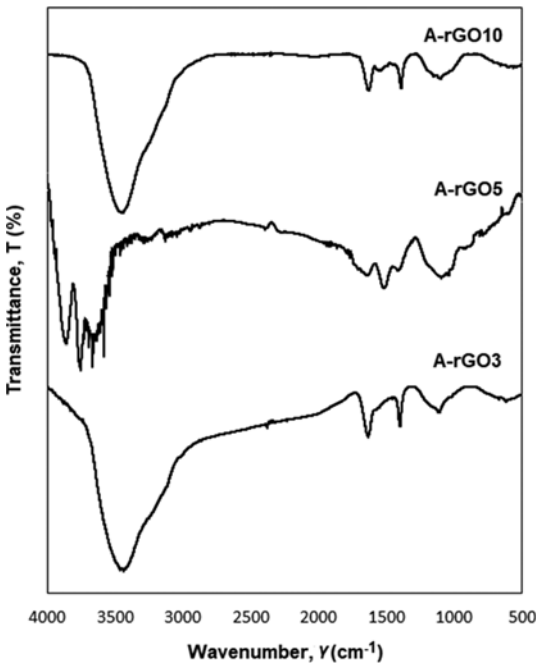

Fig. 2. FTIR spectra of A-rGO3, A-rGO5, and A-rGO10.

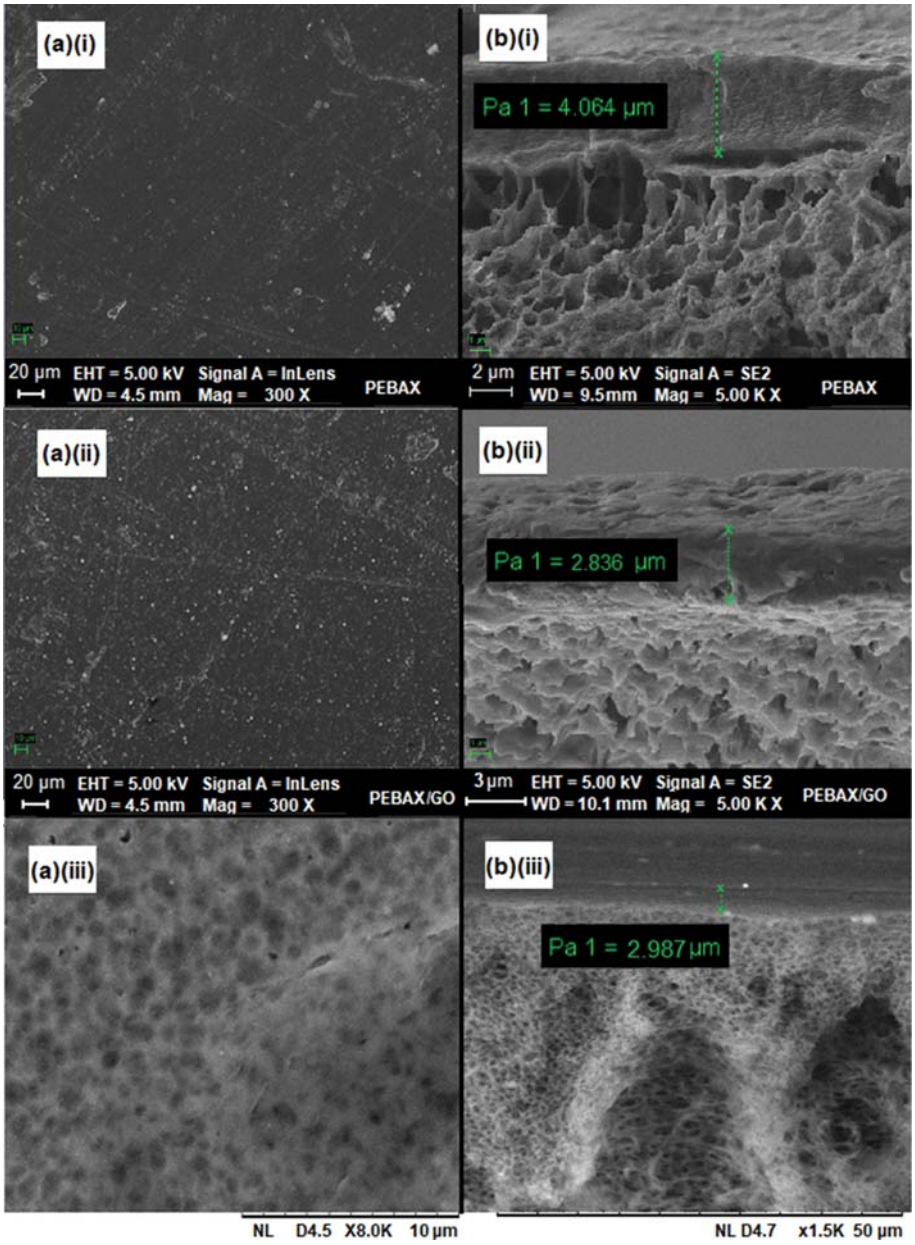

Fig. 3. SEM images of (a) surface and (b) cross-section of: (i) PEBAX; (ii) PEBAX/GO; (iii) PEBAX/A-rGO5-0.5.

absorption peak of different functional groups on graphite basal. The absorbance at 3,737 cm^{-1} represents the hydroxyl functional group. Meanwhile, the small peak between 2,500 cm^{-1} to 2,300 cm^{-1} corresponds to the carboxylic O-H. The carbonyl group and alkene bi-bound stretching were detected at 1,773 cm^{-1} and 1,649 cm^{-1}, respectively. The amine functional group absorbance was observed between 1,550 cm^{-1} and 1,650 cm^{-1} [34]. The peaks at 1,399 cm^{-1} and 1,050 cm^{-1} correspond to the stretching of C-O, which is normally observed on graphene oxide basal [35]. The C=O or COOH bond that is usually observed for GO was absent for A-rGO. This signifies the reduction of GO due to the majority removal of C=O groups by heating during the amination process [32]. The analysis result indicates that the amine group was successfully incorporated onto reduced GO.

2. Characterization of PEBAX, PEBAX/GO, and PEBAX/A-rGO5

The morphology of the fabricated PEBAX and PEBAX-based membranes was characterized using SEM. It was observed in Fig. 3(a)(i) to (iii) that the fabricated PEBAX, PEBAX/GO, and PEBAX/A-rGO5-0.5 have a smooth surface with no significant void, defect, and filler aggregation. The cross-section morphological study, as illustrated in Fig. 3(b)(i) to (iii), uncovered a homogeneous interior microstructure for all the fabricated membrane. Both the selective and porous layers were practically even in thickness and seamlessly attached. As 0.5 wt% GO and A-rGO were loaded into the PEBAX layer, the Psf support layer was being compacted evidently by the decrement in micropore size. During coating, the PEBAX solution layer penetrated the Psf pores to some extent.

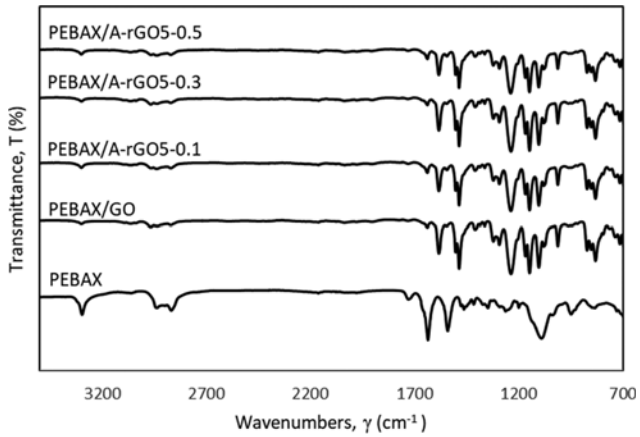

Fig. 4. FTIR spectra of the fabricated PEBAX, PEBAX/GO, and PEBAX/A-rGO5s.

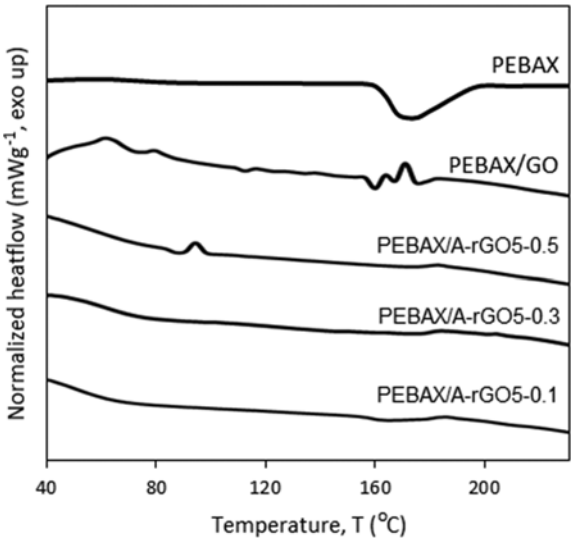

Fig. 5. DSC curves of PEBAX, PEBAX/GO, and PEBAX/A-rGO5s.

The presence of functional groups in GO and A-rGO (e.g., amine and carboxylate) enhanced the penetration process [32], which explains the thinner selective layer of PEBAX/GO and PEBAX/A-rGO5-0.5 compared to bare PEBAX.

The FTIR spectra for the fabricated membranes are shown in Fig. 4. As can be seen, the peak at 1,088 cm^{-1} of the pristine PEBAX belongs to the stretching vibration of the C-O-C group of the soft segment part of polyethylene oxide [36]. The absorbance characteristics at 1,640 cm^{-1} and 1,740 cm^{-1} correspond to H-N-C=O group and O-C=O group, respectively, which signify the availability of the hard segment of the polyamide part of PEBAX [37]. The absorbance band of N-H group in the PA block was detected at 1,548 cm^{-1} [38]. The incorporation of GO and A-rGO5 onto PEBAX shows strong and sharp peaks in the range of 800 cm^{-1} to 1,750 cm^{-1}, which were comprehensively discussed in subsection 3.1. Shifting at 1,550 cm^{-1} to 1,600 cm^{-1} for PEBAX/GO and PEBAX/A-rGO5 membranes corresponds to oxygen atoms of GO that provide several negative centers, resulting in hydrogen bonding between the H atoms of PEBAX and the O atoms of GO [32].

The DSC was performed to study the effect of A-rGO fillers on the T_g of the pristine PEBAX. The DSC curves are illustrated in Fig. 5. The broad endothermic peak ranging from 160 °C to 200 °C for pristine PEBAX is attributed to the melting of PA segment. This result was similar to that reported by Huang et al. [31]. There was a fusion of endothermic and exothermic peaks for PEBAX/GO in the range of 155 °C to 190 °C. The small endothermic peak at 163 °C corresponds to the melting temperature of PA segment. Meanwhile, the exothermic peaks at 165 °C and 170 °C, might result from the polymer matrix crystallinity in the presence of GO laminates [28]. For PEBAX/A-rGO5 MMCMs, the increasing loading of A-rGO5 did not affect the T_g since a small exothermic peak was observed at 187 °C for all fabricated MMCMs. The dispersion of A-rGO5 caused T_g to shift to a higher temperature, implying that the presence of A-rGO5 in the PEBAX matrix limits the PEBAX chains'

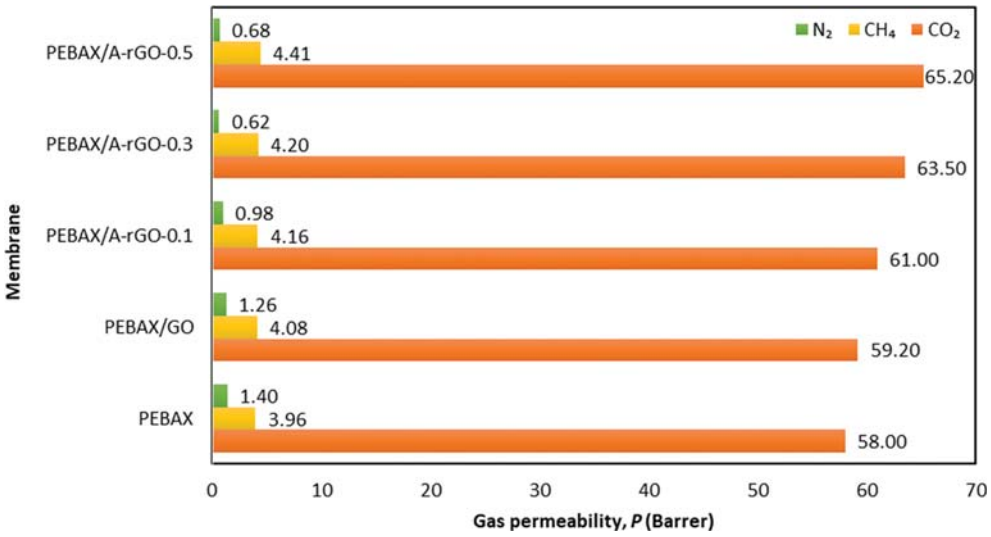

Fig. 6. Gas permeability of PEBAX, PEBAX/GO, and PEBAX/A-rGO5s.

mobility and forms a rigidified interface between PEBAX and A-rGO5 [28].

3. Gas Separation Performance

To study the effect of A-rGO loading on N_2, CH_4, and CO_2 gases separation performance, three PEBAX/A-rGO5 layer with 0.1 wt%, 0.3 wt%, and 0.5 wt% of A-rGO loading were coated on a Psf microporous support layer by a phase inversion casting. The MMCMs performance was compared with pristine PEBAX and PEBAX/GO membranes. The gases were introduced continuously in sequence into the system.

As illustrated in Fig. 6, the gas permeation order for the fabricated pristine PEBAX, PEBAX/GO, and PEBAX/A-rGO5s was CO_2>CH_4>N_2. The addition of GO filler was insignificant since only 2% permeability increment was observed compared to the pristine PEBAX with 58.00 Barrer of permeability. The permeability of CO_2 increased to 61.00 Barrer with the addition of 0.1 wt% A-rGO5 and the value increased with A-rGO5 loading achieving 65.20 Barrer permeability with 0.5 wt% of A-rGO5 loading. The CO_2 permeability reported in this study was higher than that of our previous work [32]. As shown in Fig. 6, the addition of A-rGO5 was expectedly obstructed by the CH_4 and N_2 permeation. A small increment from 4.16 Barrer to 4.41 Barrer was observed for CH_4 permeability with 0.1 wt% to 0.5 wt% A-rGO5 loadings, which were 5.1% and 11.4% higher than that of PEBAX. Meanwhile, the CH_4 permeability increased by only 3.0% for PEBAX/GO. Contrarily, the permeability of N_2 gas decreased with GO and A-rGO5 fillers. The decrement was proportional to the A-rGO5 loading. The 1.40 Barrer permeability of the PEBAX membrane was reduced to 0.68 Barrer when 0.5 wt% A-rGO5 was incorporated. It was also found in Fig. 7 that the A-rGO5 loading into PEBAX polymer significantly affects the CO_2/N_2 selectivity. The selectivity increased from 41.40 for the pristine PEBAX up to 102.40 for PEBAX/A-rGO5-0.3 and decrease with 0.5 wt% A-rGO5 loading. The A-rGO5 loading, however, was insignificant for CO_2/CH_4 selectivity.

In this study, the gas permeability order of CO_2>CH_4>N_2 does not follow the kinetic diameter of gases of CO_2>N_2>CH_4, which is in agreement with several studies [39-41]. This finding reveals that the CO_2 permeability on PEBAX/A-rGO5 was independent of the size sieving of gas molecules. The outstanding CO_2 separation by

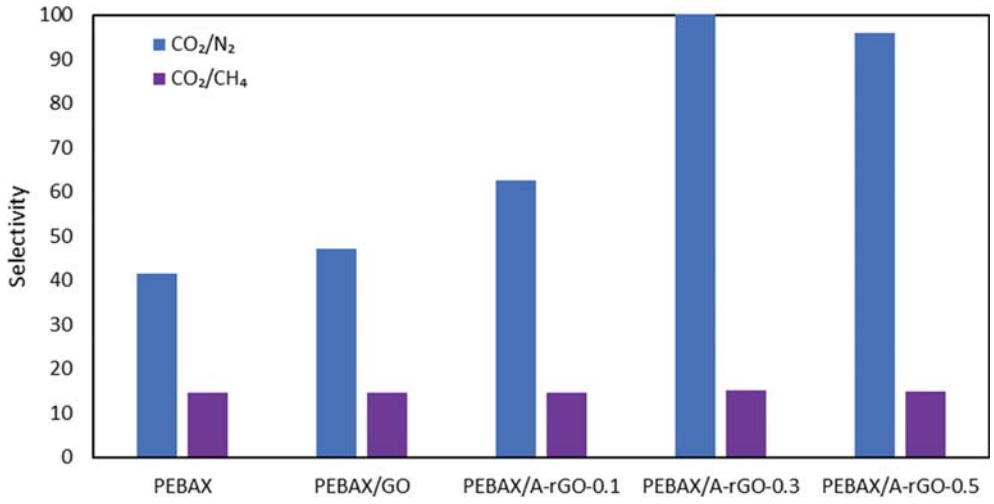

Fig. 7. Gas selectivity of PEBAX, PEBAX/GO, and PEBAX/A-rGO5s.

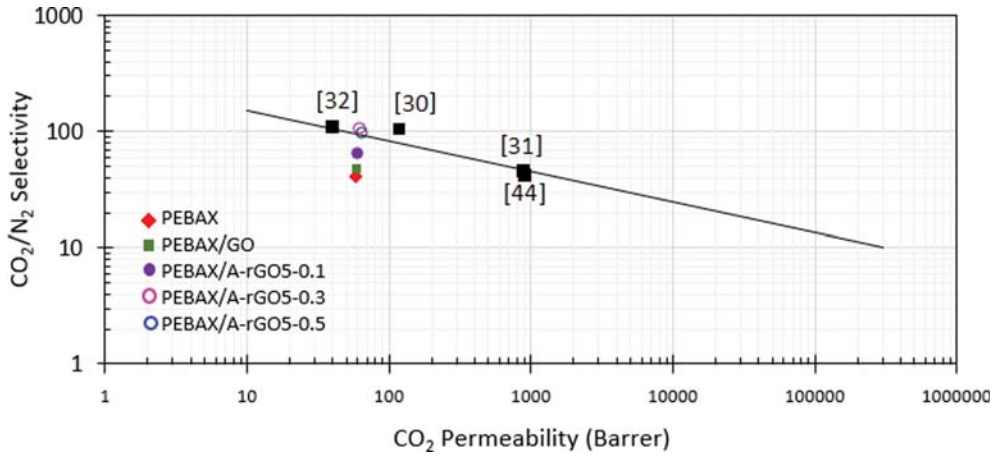

Fig. 8. Robeson plot of CO_2/N_2 selectivity in comparison with the literature [30-32,44].

the PEBAX membrane itself is due to the interaction of its polar ether oxygen to CO_2 molecules [42]. The addition of GO and A-rGO5 increased the torturous pathway, hindering the passage of CH_4 and N_2, yet allowed permeation of CO_2. The GO has an exceptional CO_2-philic feature that allowed the fastest transport of CO_2 caused by polar groups such as -OH, C-O-C, and -COOH [32,43], which explains the increment of permeability and selectivity for PEBAX/GO. The amine group of A-rGO facilitates CO_2 transportation through the membrane, which explains the higher CO_2 permeability and selectivity with A-rGO loading [32].

The 2008 Robeson upper-bound of CO_2/N_2 is plotted in Fig. 8 to display the gas separation of the fabricated membranes. The graph illustrates that the CO_2/N_2 separation performance increased with A-rGO loadings with comparable CO_2 permeability. The selectivity results of the PEBAX-based membranes from the literature were also provided as comparison [30-32,44]. The result by [31] and [44] has higher CO_2 permeability but lower selectivity. The higher permeability was due to the presence of ILs and amino groups as CO_2-philic moieties to promote an effective CO_2 permeation and enlarged interlayer spacing. However, an exceptional permeability also permits other gas molecules to pass through, resulting in the lower selectivity. In the meantime, the CO_2/N_2 selectivity of [30] and [32] was comparable to this study but deviated in CO_2 permeability. The interlayer spacing of GO-based fillers in the respective studies was almost the same (~0.34 nm), indicating similar characteristics towards providing torturous pathways for larger N_2 molecules. Since both [30] and [32] used partially reduced GO-based fillers, their crystallinity and rigidity characteristics were claimed to affect the CO_2 permeability, resulting in the observed deviations.

It is worth highlighting that the fabricated PEBAX/A-rGO5-0.3 and PEBAX/A-rGO5-0.5 membranes performance slightly surpassed the empirical Robeson 2008 upper bound for CO_2/N_2 separation. This makes the PEBAX/A-rGO5 mixed matrix composite membrane prepared in this study promising materials for CO_2 separation, specifically for post-combustion applications.

CONCLUSION

A thin selective layer of PEBAX with different A-rGO loading and coated on top of the Psf porous layer was successfully fabricated. The A-rGOs, prepared under different heating time during the amination process, showed encouraging filler properties after 5 h of heating, confirmed by XRD and FTIR analyses. The fabricated MMCMs with different A-rGO loading have a relatively good dispersion and even layer-by-layer thickness, as well as enhanced T_g. This resulted in greater performance of CO_2 permeability and CO_2/N_2 selectivity than that of PEBAX and PEBAX/GO membranes, but insignificant for CO_2/CH_4 selectivity. Since the fabricated membranes' performance is slightly above the Robeson 2008 upper bound of permeability-selectivity relation for CO_2/N_2 gas separation, they are promising alternatives for the industrial CO_2 gas separation membrane.

ACKNOWLEDGEMENTS

This research was supported by the Malaysia Ministry of Education (MOE) under the Higher Institutions' Centre of Excellence Grant (HICOE) [grant number R.J090301.7851.4J431] and Universiti Teknologi Malaysia under the Collaborative Research Grant (CRG National) [grant number R.J130000.7351.4B474].

REFERENCES

1. S. Loeb and S. Sourirajan, *Adv. Chem.*, **38**, 117 (1962).
2. T. Li, Y. Pan, K.-V. Peinemann and Z. Lai, *J. Membr. Sci.*, **425-426**, 235 (2013).
3. M. Vinoba, M. Bhagiyalakshmi, Y. Alqaheem, A. A. Alomair, A. Pérez and M. S. Rana, *Sep. Purif. Technol.*, **188**, 431 (2017).
4. L. M. Robeson, *J. Membr. Sci.*, **320**, 390 (2008).
5. Y. Xiao, B. T. Low, S. S. Hosseini, T. S. Chung and D. R. Paul, *Prog. Polym. Sci.*, **34**, 561 (2009).
6. M. Zhang, L. Deng, D. Xiang, B. Cao, S. Hosseini and P. Li, *Processes*, **7**, 51 (2019).
7. N. N. R. Ahmad, C. P. Leo, A. W. Mohammad and A. L. Ahmad, *Micropor. Mesopor. Mater.*, **244**, 21 (2017).
8. M. G. Miricioiu, C. Iacob, G. Nechifor and V.-C. Niculescu, *Front. Chem.*, **7**, 332 (2019).
9. Z. Hamrahi and A. Kargari, *Sep. Purif. Technol.*, **52**, 544 (2017).
10. Y. Zhang, H. Wang, W. Yu, J. Shi and H. Shi, *J. Membr. Sci.*, **564**, 916 (2018).
11. H. Asghar, A. Ilyas, Z. Tahir, X. Li and A. L. Khan, *Sep. Purif. Technol.*, **203**, 233 (2018).
12. H. A. Mannan, D. F. Mohshim, H. Mukhtar, T. Murugesan, Z. Man and M. A. Bustam, *J. Ind. Eng. Chem.*, **54**, 98 (2017).
13. M. Mubashir, Y. F. Yeong, K. K. Lau and T. L. Chew, *Polym. Test.*, **73**, 1 (2019).
14. Z. Tong and W. S. W. Ho, *J. Membr. Sci.*, **543**, 202 (2017).
15. S. Majumdar, G. Tokay, V. Martin-Gil, J. Campbell, R. Castro-Muñoz, M. Z. Ahmad and V. Fila, *Sep. Purif. Technol.*, **238**, 116411 (2020).
16. H. Sun, T. Wang, Y. Xu, W. Gao, P. Li and Q. J. Niu, *Sep. Purif. Technol.*, **177**, 327 (2017).
17. E. Ahmadpour, A. A. Shamsabadi, R. M. Behbahani, M. Aghajani and A. Kargari, *J. Nat. Gas Eng.*, **21**, 518 (2014).
18. R. Selyanchyn, M. Ariyoshi and S. Fujikawa, *Membranes*, **8**, 121 (2018).
19. K. W. Jung and S. W. Kang, *Sci. Rep.*, **9**, 11454 (2019).
20. A. Brunetti, M. Cersosimo, J. S. Kim, G. Dong and E. Fontananova, *Int. J. Greenh. Gas Con.*, **61**, 16 (2017).
21. Y. Ying, Y. Cheng, S. B. Peh, G. Liu, B. B. Shah, L. Zhai and D. Zhao, *J. Membr. Sci.*, **582**, 103 (2019).
22. S. Shahid and K. Nijmeijer, *Sep. Purif. Technol.*, **189**, 90 (2017).
23. Q. Xin, Y. Zhang, Y. Shi, H. Ye, L. Lin, X, Ding, Y. Zhang, H. Wu and Z. Jiang *J. Membr. Sci.*, **514**, 73 (2016).
24. D. Qadir, H. Mukhtar and L. K. Keong, *Procedia Eng.*, **148**, 588 (2016).
25. K. Goh, H. E. Karahan, L. Wei, T.-H. Bae, A. G. Fene, R. Wang and Y. Chen, *Carbon*, **109**, 694 (2016).
26. K. Goh, J. K. Heising, Y. Yuan, H. E. Karahan, L. Wei, S. Zhai, J.-X. Koh, N. M. Htin, F. Zhang, R. Wang, A. G. Fene, M. Dekker, F. Dehghani and Y. Chen, *ACS Appl. Mater. Interfaces*, **8**, 9994 (2016).
27. X. Li, L. Ma, H. Zhang, S. Wang, Z. Jiang, R. Guo, H. Wu, X. Cao, J. Yang and B. Wang, *J. Membr. Sci.*, **479**, 1 (2015).

28. X. Li, Y. Cheng, H. Zhang, S. Wang, Z. Jiang, R. Guo and H. Wu, *ACS Appl. Mater. Interfaces*, **7**, 5528 (2015).
29. Y. Shen, H. Wang, J. Liu and Y. Zhang, *ACS Sustain. Chem. Eng.*, **3**, 1819 (2015).
30. G. Dong, J. Hou, J. Wang, Y. Zhang, V. Chen and J. Liu, *J. Membr. Sci.*, **520**, 860 (2016).
31. G. Huang, A. P. Isfahani, A. Muchtar, K. Sakurai, B. B. Shrestha, D. Qin, D. Yamaguchi, E. Sivaniah and B. Ghalei, *J. Membr. Sci.*, **565**, 370 (2018).
32. S. A. Mohammed, A. M. Nasir, F. Aziz, G. Kumar, W. Sallehhudin, J. Jaafar, W. J. Lau, N. Yusof, W. N. W. Salleh and A. F. Ismail, *Sep. Purif. Technol.*, **223**, 142 (2019).
33. H.-H. Huang, K. K. H. De Silva, G. R. A. Kumara and M. Yoshimura, *Sci. Rep.*, **8**, 6849 (2018).
34. N. Hu, Z. Yang, Y. Wang, L. Zhang, Y. Wang, X. Huang, H. Wei, L. Wei and Y. Zhang, *Nanotechnology*, **25**, 025502 (2013).
35. D. Konios, M. M. Stylianakis, E. Stratakis and E. Kymakis, *J. Colloid Interface Sci.*, **430**, 108 (2014).
36. J. H. Kim and Y. M. Lee, *J. Membr. Sci.*, **193**, 209 (2001).
37. A. Ghadimi, M. Amirilargani, T. Mohammadi, N. Kasiri and B. Sadatnia, *J. Membr. Sci.*, **458**, 14 (2014).
38. N. Azizi, M. Arzani, H. R. Mahdavi and T. Mohammadi, *Korean J. Chem. Eng.*, **34**, 2459 (2017).
39. H. W. Kim, H. W. Yoon, B. M. Yoo, J. S. Park, K. L. Gleason, B. D. Freeman and H. B. Park, *Chem. Commun.*, **50**, 13563 (2014).
40. M. Karunakaran, R. Shevate, M. Kumar and K. V. Peinemann, *Chem. Commun.*, **51**, 14187 (2015).
41. J. Shen, G. Liu, K. Huang, W. Jin, K.-R. Lee and N. Xu, *Angew Chem. Int. Ed.*, **54**, 578 (2015).
42. M. M. Rahman, V. Filiz, S. Shishatskiy, C. Abetz, S. Neumann, S. Bolmer, M. M. Khan and V. Abetz, *J. Membr. Sci.*, **437**, 286 (2013).
43. Y. Alqaheem, A. Alomair, M. Vinoba and A. Pérez, *Int. J. Polym. Sci.*, **2017** (2017).
44. J. Zhang, Q. Xin, X. Li, M. Yun, R. Xui, S. Wang, Y. Li, L. Lin, X. Ding, H. Ye and Y. Zhang, *J. Membr. Sci.*, **570-571**, 343 (2019).